Structure optimization design of high-temperature, high-pressure nuclear power valve

Wei Li [ab*], Enda Li [a], Hao Chang [a], Jianrui Liu [a*], Chang Li [a] & Xingyuan Wang [c]

[a] Research Center of Fluid Machinery Engineering and Technology, Jiangsu University, Zhenjiang, China. lwjiangda@ujs.edu.cn, 834049773@qq.com, changhao1514@163.com, ljrwjj@126.com, lichang985@163.com
[b] Institute of Fluid Engineering Equipment Technology, Jiangsu University, Zhenjiang, China. lwjiangda@ujs.edu.cn
[c] Kunming Branch of 705 Research Institute of China Shipping Heavy Industry Group Co., Ltd, Kunming, China. wangxingyuan755@sohu.com

Abstract

The nuclear power valve is an important piece of equipment in any nuclear power system. The finite element method was used in this study to analyze the strength and rigidity of the high-temperature and high-pressure nuclear gate valve. The structural characteristics were optimized as per the parameters that affect the strength of the valve body. Fluid-solid coupling technology was utilized to investigate the temperature, deformation, and stress distributions in the structure. A high stress concentration was observed in the initial design; the maximum equivalent stress exceeded the allowable range. Three optimization methods were deployed in efforts to improve the stress distribution. The stress distribution was found to be more uniform post-optimization and the gate valve structure of all three schemes tested met the relevant stress requirements. The optimal scheme was then determined by further comparison. The results presented here may provide a theoretical reference for the optimization of nuclear power valve designs.

Keywords: high temperature; high pressure; valve; structure optimization; fluid-solid thermal coupling.

Optimización de la estructura de las válvulas nucleares de alta presión

Resumen

La válvula de energía nuclear es un equipo importante en cualquier sistema de energía nuclear. El método de elementos finitos se utilizó en este estudio para analizar la resistencia y la rigidez de la válvula de compuerta nuclear de alta temperatura y alta presión. Las características estructurales se optimizaron según los parámetros que afectan la resistencia del cuerpo de la válvula. La tecnología de acoplamiento fluido-sólido se utilizó para investigar la temperatura, la deformación y las distribuciones de tensiones en la estructura. Se observó una alta concentración de tensiones en el diseño inicial; El esfuerzo equivalente máximo excedió el rango permitido. Se desplegaron tres métodos de optimización en un esfuerzo por mejorar la distribución del estrés. Se encontró que la distribución de la tensión era más uniforme después de la optimización y la estructura de la válvula de compuerta de los tres esquemas probados cumplía con los requisitos de tensión relevantes. El esquema óptimo se determinó luego mediante una comparación adicional. Los resultados presentados aquí pueden proporcionar una referencia teórica para la optimización de los diseños de válvulas de energía nuclear.

Palabras clave: alta temperatura; alta presión; válvula; optimización de estructura; acoplamiento térmico fluido-sólido.

1. Introduction

The nuclear power gate valve, which is installed in nuclear and conventional islands in nuclear power station and power station auxiliary facilities, is a key component of the nuclear power plant system [1-3]. It is used to control medium pressure, temperature, flow direction, and flow rate while safeguarding the pressure vessel [4,5]. Clean, renewable energy (e.g., wind power) is rapidly becoming a priority as the national economy progresses; the market

demand for nuclear power valves is expected to continually increase [6]. However, the high pressure and high temperature of the medium affect the strength and stiffness of the valve and thus drive down its sealing performance. To prevent structural failure due to deformation of the gate valve or any stress exceeding the allowable value, it is necessary to optimize the valve design by effectively analyzing its fluid−solid coupling.

The self-excited vibration generated by the nonlinear characteristics of the coupled spool movement and fluid dynamics create instability in the system, which in turn degrades performance and damages the hardware. Improper system parameters are generally the culprit. The pressure control valve design can thus be optimized according to its stability, as-proposed by Jian [7]. The stable boundary in the parameter space was determined via numerical simulation; the pressure control valve was then optimized by particle swarm optimization algorithm with the stable boundary as a constraint. Samad [8] analyzed the vibration characteristics of control valves of various shapes under the action of fluid exciting force to find that the vibration amplitude of a circular valve is lower than that of a flat or steep valve. Anelina[9] examined the stress and strain characteristics of a steam valve to find that changes in the time variable and non-uniform temperature field alter the local stress leading to metal fatigue.

There have been many other valuable contributions to the literature. Zhao et al.[10] used the finite element method to observe the effects of current on the dynamic characteristics and power loss of a high-speed solenoid valve; a decrease in driving current was found to deteriorate the high-speed solenoid valve open response, but the power loss can be reduced to enhance the valve's energy utilization rate. When the appropriate current is maintained, it is possible to achieve an optimal balance between the opening response time and the energy distribution. Liu et al. [11] studied a butterfly valve installed in nuclear power plant pressurized water reactor circulating water systems; they established a computational fluid dynamics (CFD) model coupled with multi-phase, cavitation, and discrete phase properties. Numerical simulations were run to validate the coupling model according to cavitation, particle erosion, and flow coefficient characteristics. The effect of erosion was found to grow more severe as inlet pressure increases.

The gate valve has more strict sealing requirements than the butterfly valve and potentially higher medium pressure and temperature. Hu et al. [12] used a three-dimensional (3D) steady-state CFD method to simulate the conjugate heat transfer of an underwater gate valve. They combined various turbulence models and near wall processes to secure a k-ε turbulence model combined with low Reynolds number that well resolves the underwater conjugate heat transfer problem. Lin [13] and Huang [14] analyzed the resistance characteristics and internal flow characteristics of gate valves with different inlet speeds by CFD with 8 relative opening schemes. They found that the pressure coefficients of upstream and downstream gate valve pipes are basically the

same at different inlet speeds, but when the relative opening is 2/8, the internal flow is chaotic and there is a high-speed jet flow. The pressure distribution on the valve is uneven, which severely affects its sealing performance.

Lin [15] adopted the Euler Lagrange simulation method to observe the gas-solid flow characteristics and erosion performance of horizontal and vertical gate valves. They found only slight differences between the gas flow characteristics and the flow coefficient in two cases for all open degrees and Stokes numbers. However, as Stokes number increased, the difference between the two kinds of trajectories grew increasingly obvious as did the differences in erosion distribution. Tomarov et al. [16] studied the corrosion resistance nuclear power plant valves, established possible cavitation conditions, and proffered realistic proposals to prevent valve damage. The gate valve is sealed through the valve seat and the gate, so the interaction of the valve seat and the gate markedly affects the seal.

Kolesnikov [17] and Wu [18] conducted finite element analysis on the fracture toughness of the valve body and the interaction of the contact between the gate and the valve seat. The contact force interaction must be small enough to prevent failure, but decreasing the contact interactions increases the risk of leakage - it is crucial to ensure the appropriate interaction force. Lin [19] applied a decoupling analysis method to establish a unified fluid solid coupling calculation model for the fluid structure interaction problem of air pressure seal valves. Based on the fluid solid coupling model, finite element analysis and CFD were applied to simulate the pneumatic seal valve for analysis.

Previous research on gate valves has mostly centered on vibration characteristics, sealing performance, and flow field analysis. However, the working medium, temperature, pressure, load, and other conditions related to the nuclear power plant valve's high-temperature and high-pressure environment are more severe than those of the conventional gate valve. It is yet necessary to carry out fluid-solid thermal coupling to optimize the stability of valves utilized in nuclear power plants and other similar facilities. There have been relatively few studies on structural optimization and fluid solid heat coupling of high-temperature and high-pressure gate valves.

The deformation of the valve body as well as the size and distribution of the equivalent stress under test pressure and working pressure conditions were examined in this study by numerical simulation. The design variables, state variables, and objective functions were input to the optimization design module of the ANSYS Workbench to design the body structure. Fluid-solid heat coupling was utilized to investigate the temperature, deformation, and stress distribution of the gate valve under working conditions. The effects of various design parameters on the stress and deformation of the valve body were observed accordingly. The optimization scheme as-determined by this analysis was found to improve the stress and strain distribution of the valve body. The results presented below may serve as a workable theoretical reference for the optimization high-temperature and high-pressure gate valve designs.

Table 1.
Working parameters of gate valve.

Nominal diameter	Working pressure	Working temperature	Working medium	Medium velocity
150 mm	15 MPa	330 ℃	Boronizing water	10 m/s

Source: The Authors.

Table 2.
Gate valve component materials.

Part name	Material brand
Valve body	F6a
Seat sealing surface	PT1101
Gate sealing surface	PT1102
Stem	3Cr13
Gate	F6a
Bolt	35CrMo
Valve cover	F6a
medium flange seal ring	Winding gasket (containing asbestos)
Filler	Graphite composite

Source: The Authors.

Figure 1. Geometric structure of valve body.
Source: The Authors.

Figure 2. Gate valve 3D model.
Source: The Authors.

2. Working parameters of gate valve

The parameter ranges of the primary loop of the PWR nuclear power plant are as follows. The working pressure is about 15 MPa, the inlet temperature of the coolant in the reactor is 280 ℃-300 ℃, the outlet temperature of the reactor is 310 ℃-330 ℃, and the increase of the import and export temperature is 30 ℃-40 ℃. The maximum average temperature difference allowed by the reactor coolant is 17 ℃-25 ℃ and the design temperature of the reactor is 350 ℃. The parameters of the gate valve designed in this study are listed in Table 1.

The GB/T12224-2005 states that the nominal pressure of the gate valve is the design pressure of 25 MPa. The material of each part of the valve is determined by the working parameters of the device (Table 2).

3. Gate valve calculation model

The outer diameter of the main channel of the gate valve initial model is D_1=115 mm, the outer diameter of the middle cavity is D_2=160 mm, the distance between the upper part of the seat and the central line of the main channel is D_3=59 mm, the chamfering size at the upper part of the seat is D_4=50 mm, and the chamfering size of the seat outer circumference is D_5=12 mm. These main body structure parameters are also shown in Fig. 1.

An effective 3D solid model of the gate valve accurately reflects the actual working conditions of the structure. The model should also be simplified to the greatest extent possible without sacrificing calculation accuracy.

The pressure boundary of the gate valve mainly includes valve body, valve cover, and gate (Fig. 2). These three components, as a whole, bear internal pressure in the device. They are considered as a whole in the finite element model and the connection bolts between them are ignored. This allows for simplification of features that do not affect the
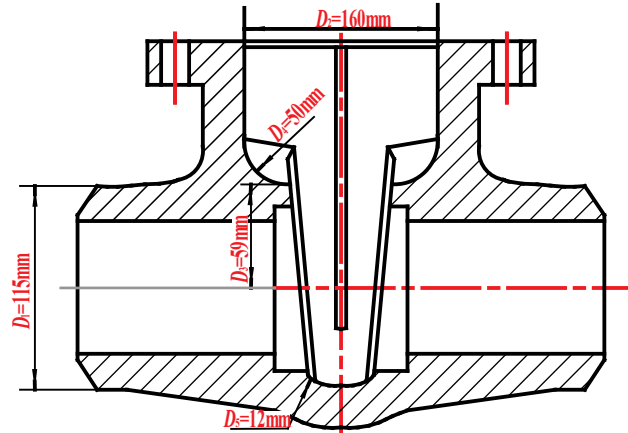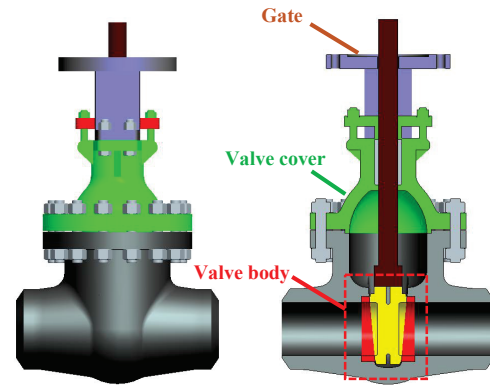
overall performance of the gate valve while ignoring some unnecessary chamfering. The 3D gate valve model used in this study was drawn in Pro/E software as shown in Fig. 2.

4. Structure optimization design method

Structural optimization design is an efficient and convenient approach to analyses such as the one conducted in this study. First, $x = (x_1, x_2,...,x_n)^T$ is set as a vector in n-dimensional Euclidean space R^n and $f(x)$ as a pre-defined function[20-22]. Then the optimization problem proceeds by obtaining vector x under the constraint conditions $ci(x)$ and $cj(x)$, which makes the function $f(x)$ a maximum (or minimum) value. This can be expressed as follows:

$$\min f(x)$$
$$s.t.\ c_i(x)=0 \qquad i=1, 2, …, m \qquad (1)$$
$$c_j(x) \geq 0 \qquad j=m+1, m+2, …, n$$

where $f(x)$ is objective function, $ci(x)$ is equality constraint condition, $cj(x)$ is inequality constraint condition, x is design variable, $f(x)$, $ci(x)$ and $cj(x)$ are two order continuous differentiable functions defined in space R^n.

150

5. Coupling analysis model

5.1. Fluid-solid coupling calculation model

In this study, Workbench integrated in Ansys17.1 was used for fluid-solid thermal coupling of nuclear power valve. The fluid calculation domain was applied in Fluent software integrated with the fluid-solid coupling module in Workbench for numerical simulation. Static Structural software (ANSYS) was used to calculate the solid domain.

"Fluid-solid coupling" refers to the deformation or movement of a solid medium under the action of load. The deformation or movement in turn affects the medium, thereby changing the distribution and magnitude of the load acting upon it.

The finite element equation for fluid-solid coupling is:

$$\begin{cases} AU + BUU + CP = DU = E + F \\ GU = H \\ M\delta'' + C\delta' + K\delta = P \end{cases} \tag{2}$$

where U, P are the column vectors composed of all the nodes in the whole domain and $U= [UVW]^{T}$.

Each coefficient matrix is superimposed by the corresponding coefficient matrix of all the elements in the whole domain:

$$A=\Sigma A^e, B=\Sigma B^e, C=\Sigma C^e, D=\Sigma D^e, E=\Sigma E^e, F=\Sigma F^e, G=\Sigma G^e, H=\Sigma H^e \tag{3}$$

where A^e is the mass matrix, B^e is the convective matrix, C^e is the pressure matrix, D^e is the loss matrix, E^e and F^e are volume force matrices, G^e is the continuous matrix, H^e is the boundary velocity vector, δ'', δ', and δ are the acceleration, velocity, and structure stress column vector, respectively, M is the mass matrix, K is the stiffness matrix, and C is the damping matrix.

5.2. Temperature field calculation model

The temperature field is the temperature distribution of each part in the designated area; it also denotes the temperature distribution of each point in every moment. Solids and fluids conduct heat. The convection heat transfer phenomenon between a given fluid and solid is mainly attributable to the basic law of heat transfer.

(1) Heat conduction differential equation

In the Cartesian coordinate system, for any point in the heat conduction object (x, y, z), the general form of the 3D unsteady heat conduction differential equation is:

$$\rho c \frac{\partial t}{\partial \tau} = \frac{\partial}{\partial x}\left(\lambda \frac{\partial t}{\partial x}\right) + \frac{\partial}{\partial y}\left(\lambda \frac{\partial t}{\partial y}\right) + \frac{\partial}{\partial z}\left(\lambda \frac{\partial t}{\partial z}\right) + \dot{\Phi} \tag{4}$$

where ρ is density (kg/m³), c is specific heat (J/(kg·K)), λ is thermal conductivity (W/(m·K)), and $\dot{\Phi}$ is the unit volume heating rate.

The continuous differential equation is:

$$\frac{\partial \rho}{\partial \tau} + \frac{\partial(\rho u)}{\partial x} + \frac{\partial(\rho v)}{\partial y} + \frac{\partial(\rho w)}{\partial z} = 0 \tag{5}$$

The motion differential equation is:

$$\frac{\partial}{\partial \tau}(\rho u_i) + \frac{\partial}{\partial x_j}(\rho u_i u_j) = -\frac{\partial p}{\partial x_i} + \frac{\partial \tau_{ij}}{\partial c_j} + \rho g_i + F_i \tag{6}$$

The energy differential equation is:

$$u_x \frac{\partial T}{\partial x} + u_y \frac{\partial T}{\partial y} + u_z \frac{\partial T}{\partial z} = \frac{\lambda}{c_p \rho}\left(\frac{\partial^2 T}{\partial x^2} + \frac{\partial^2 T}{\partial y^2} + \frac{\partial^2 T}{\partial z^2}\right) \tag{7}$$

6. Finite element analysis of valve body strength and stiffness

6.1. Grid division, constraint and load condition

The model is divided by an unstructured grid. The driving mechanism on the upper part of the connecting frame is not included in the calculation, as shown in Fig. 3. The grid partition software in ANSYS Workbench was used to divide the complex model and automatically encrypt its small parts. After division, the number of mesh elements was 266161 and the number of nodes was 444540.

Mesh independence verification was performed on the solid domain under working pressure of 25 MPa. The maximum deformation was used as a criterion to judge the grid independence.

When the total mesh elements of the computational domains was 2.66 million, the maximum deformation was stable with further increase in grid number and the error was less than 1%. This meets mesh-independence testing requirements.
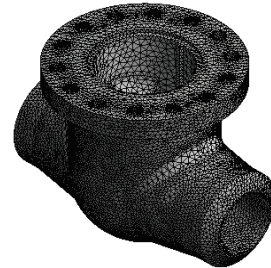

Figure 3. Valve body mesh division.
Source: The Authors.

Tabel.3
Comparison of the deformation with different mesh elements.

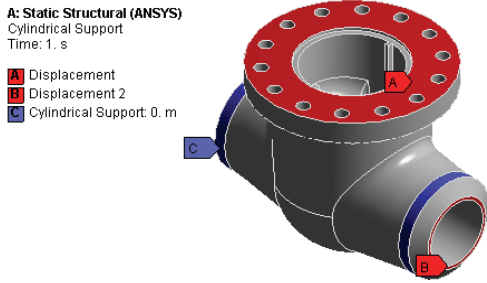| Grid scheme	Mesh elements	Maximum deformation (mm)
A	218642	0.05319
B	237652	0.05324
C	266161	0.05337

Source: The Authors.

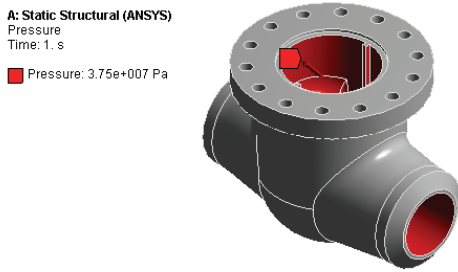Figure 4. Restriction of valve body.
Source: The Authors.

Figure 5. Application of internal load on valve body
Source: The Authors.

Axial displacement constraints were imposed on both ends of the valve body as they are welded to the pipe. The middle flange was connected to the cover of the valve and a vertical displacement constraint was applied to the end face of the flange. A cylindrical constraint was applied to the circumference of the two ends of the body to restrict the tangential and axial movement of the valve. The constrained body model is shown in Fig. 4.

According GB/T13927-1992, the test medium of the shell pressure of industrial valves is usually water or air. The pressure of the system must reach (or exceed) the specified test pressure during a shell test to reveal whether the tested valve meets the given holding pressure performance requirements. According to the regulations, 1.5 times the nominal pressure (37.5 MPa) was taken as the test pressure. The test medium was water at normal temperature. The effect of the bolt preloading force and the weight of the valve body was ignored. The resulting valve body model after load application is shown in Fig. 5.

6.2. Finite element analysis of valve body strength and stiffness

GB/T13927-1992 stipulates that the pressure wall experiences no visible leakage nor does the shell present structural damage in the test process. The cavity deformation body is usually controlled in the range of $0.001DN$, otherwise the seal will be damaged by force deformation. The nominal diameter of the valve is 150 mm, so the allowable deformation is 0.15 mm. Under the experimental pressure of 37.5 MPa, after numerical simulation, the maximum deformation of the valve body was 0.076 mm and located on the sides of the middle cavity and main channel axis. The

shape of the valve in this case is very simple (approximately cylindrical) and easily deformed, as shown in Fig. 6(a).

The simulation results altogether indicate that the body structure meets the given stiffness requirements. As shown in Fig. 6(b), the maximum equivalent stress of the valve body is 219.2 MPa under the test pressure of 37.5 MPa and is located at the chamfer of the seat. There is a stress concentration at this point, and the allowable stress of the material is [s]=210 MPa, so the maximum equivalent stress of the valve body is beyond the allowable stress range of the material.

The deformation and equivalent stress of the valve body under the working pressure of 25 MPa were obtained as shown in Fig. 7. The maximum deformation of the valve body was found to be 0.053 mm and the maximum equivalent
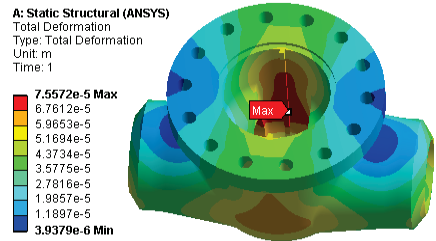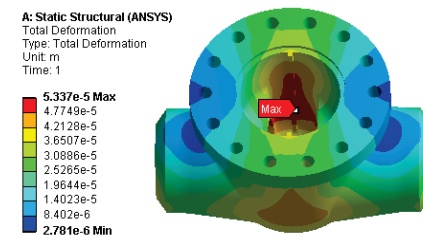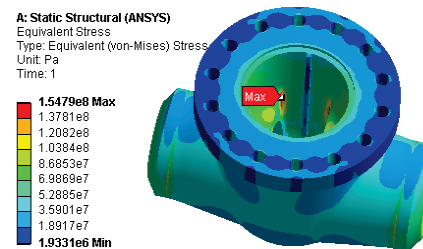

(a) Deformation
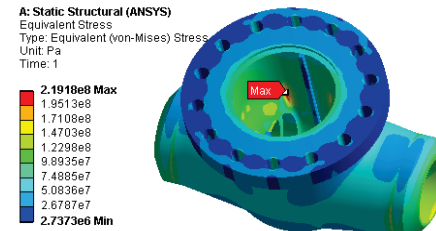
(b) Equivalent stress
Figure 6. Deformation and equivalent stress contour chart of valve body under test pressure.
Source: The Authors.

(a)   Deformation

(b) Equivalent stress
Figure 7. Deformation and equivalent stress contour chart of valve body under working pressure.
Source: The Authors.

stress is 154.8 MPa, which meet the relevant stiffness and strength requirements. However, stress concentration persisted at the chamfer of the seat part at this point. It is necessary to improve the stress concentration of the valve body to ensure the optimal strength, safety, and economy of the device.

7. Optimization of valve body structure

7.1. Selection of variables and objective functions

As shown in Fig. 6, the maximum equivalent stress of valve body was identified at the chamfer of valve seat part. The stress at the seat part is large as is the deformation on both sides of the valve body, but the stiffness requirements are still met in this case. Therefore, the parameters of the valve seat and the section structure of the middle cavity can be considered optimization variables when optimizing the valve body structure.

The selected design variables must have an upper and lower bound. The ranges of optimum design variables in this study are shown in Table 4. The mass, which affects the economy of the device, was also set as a state variable.

The objective function is the expression of a certain performance index characterized by design variables. The proper objective function is directly related to the optimization of the valve body design, and is an expression of a certain performance index under the given design variables. The objective function must be selected properly to effectively optimize the valve body. Here, in order to make the equivalent stress of the valve body smaller than the allowable stress of the material, standardize the stress distribution of the valve body, and eliminate the stress concentration phenomenon, the maximum equivalent stress

of the valve body was set as objective function. This allowed us to achieve the allowable stress range under the design and state variable constraints.

7.2. Effects of design parameters on valve body stress and deformation

The response surface was optimized with the Design Explorer optimization module in ANSYS Workbench. The response diagram of the maximum equivalent stress of certain design variables on the valve body is shown in Fig. 8. The maximum equivalent stress of the valve body was found to first increase slowly with increase in D_2, then decrease rapidly once D_2 exceeded 159 mm. The maximum equivalent stress and amplitude decreased as D_5 increased. There was no obvious change in the maximum equivalent stress as D_1 increased; the contour indicates that it has little influence on the maximum equivalent stress of the valve body. The response graphs of other design variables are similar to that of D_1.

A response diagram for the maximum deformation of various design variables on the valve body was obtained as shown in Fig. 9. The maximum deformation of the valve body increased, though only slightly, as D_1 increased.

Table 4.
Range of value for design variables.

Design variable	Initial value /mm	Maximum value/mm	Minimum value /mm
D_1	115	118	112
D_2	160	162	155
D_3	59	62	56
D_4	50	52	48
D_5	12	15	6

Source: The Authors.

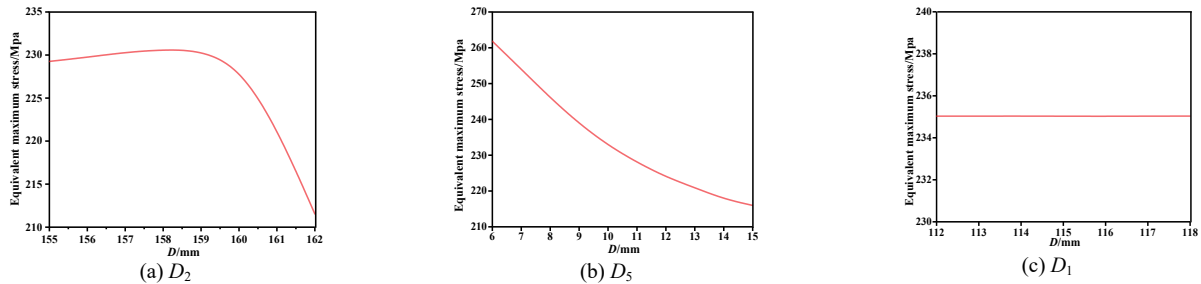(a) D_2 (b) D_5 (c) D_1

Figure 8. Response diagram of design variable to maximum valve body equivalent stress.
Source: The Authors.

(a) D_1 (b) D_2

Figure 9. Response diagram of design variable to maximum valve body deformation.
Source: The Authors.

The maximum deformation of the valve body decreased as D_2 increased. The responses of the other design variables to the maximum deformation of the valve body were similar to that of D_2. Changes in design variable size appear to have little influence on the maximum deformation of the valve body and thus do not markedly affect the sealing performance of the valve.

7.3. Design space and sensitivity analysis of stress intensity

The maximum equivalent stress value of the valve body was minimized in this case due to the interactions among all optimization variables rather than the single function of a parameter. The solution obtained is the global solution within the constraint range. The calculated stress intensity design space is shown in Fig. 10 and the parameter sensitivity analysis is shown in Fig. 11. With in the specified design variables, changes in D_2 appear to significantly influence the maximum deformation, the maximum equivalent stress, and the mass of the valve body. Changes in D_5 significantly influence the maximum equivalent stress and changes in D_1 significantly influence on the mass.

(a) D_2 and D_3

(b) D_2 and D_5

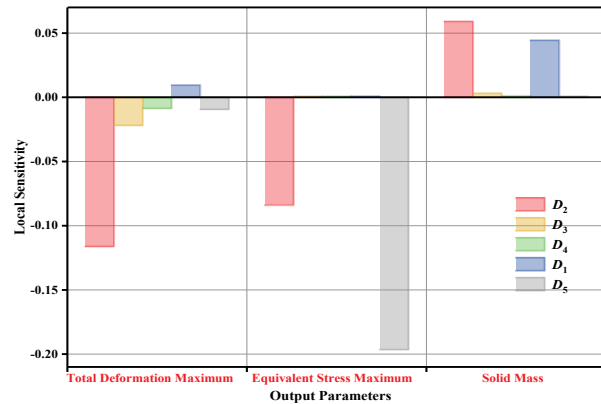Figure 10. Stress intensity design space.
Source: The Authors.

Figure 11. Sensitivity analysis of design parameters.
Source: The Authors.

7.4. Optimization results and analysis

The limitation range of each geometric parameter is listed in Table 4. The interaction of each geometric parameter of the valve on the maximum equivalent stress and the maximum deformation was determined through the objective function and response surface analysis (Section 7). The value range of each parameter was further clarified as discussed above and three optimization schemes were determined accordingly.

As shown in Fig. 8 (a), the equivalent stress and deformation are minimal when the diameter of D_2 reaches the maximum allowable value of 162 mm. As shown in Figg. 10 and 11, changes in D_2 markedly influence the maximum deformation, maximum equivalent stress, and mass of the valve body. The D_2 value of the three schemes was thus selected as 162 mm. The maximum equivalent stress also decreases as D_5 increases; D_5 was set to 12 mm, 14 mm, and 15 mm in this test. The value range of D_1, which significantly influences mass, was set to 112-118 mm.

Considering the matching of geometric dimensions, the value ranges, and the impact on the mass, the three optimization schemes were defined by 113 mm, 114 mm, and 116 mm values, respectively. Similarly, D_3 and D_4 were set to different values in an equilibrium relationship. The three schemes tested in this study were thus obtained by changing the values of D_1, D_3, D_4, and D_5. The variables that affect the strength of the valve body were optimized in the finite element program according to these three optimization schemes (Table 5).

Under the same material, mesh generation, constraint, and load experimental conditions as the initial design, three optimization models were analyzed by finite element method to obtain the equivalent stress and deformation cloud maps shown in Figs. 12-14. The original stress concentration point was substantially reduced and the stress distribution grew more uniform after the optimization. The maximum equivalent stress of the optimized valve body was located at the seat chamfering (Scheme 1) or the seat top (Scheme 2, Scheme 3). The maximum equivalent stress was less below the material allowable stress, which in practice would ensure a strong valve body satisfying the given work requirements.
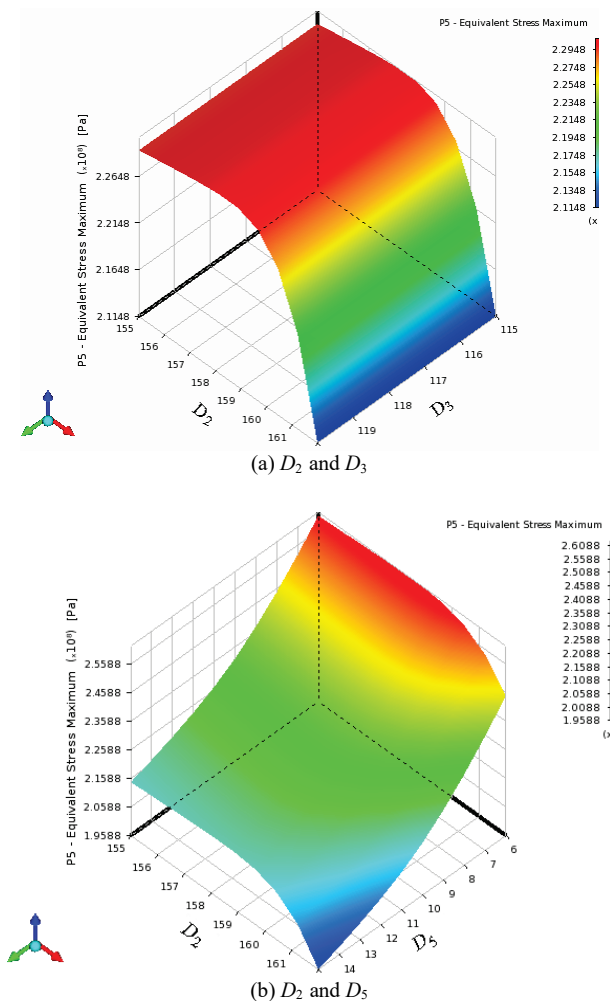
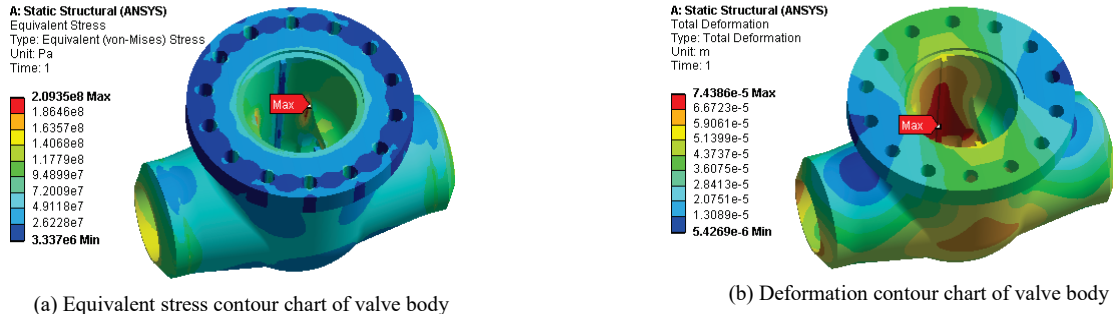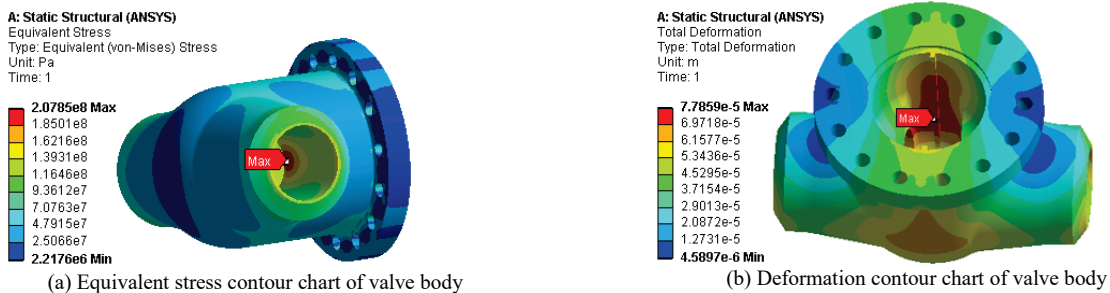(a) Equivalent stress contour chart of valve body

(b) Deformation contour chart of valve body

Figure 12. Equivalent stress and deformation contour chart of Scheme 1.
Source: The Authors.

(a) Equivalent stress contour chart of valve body

(b) Deformation contour chart of valve body

Figure 13. Equivalent stress and deformation contour chart of Scheme 2.
Source: The Authors.

(a) Equivalent stress contour chart of valve body

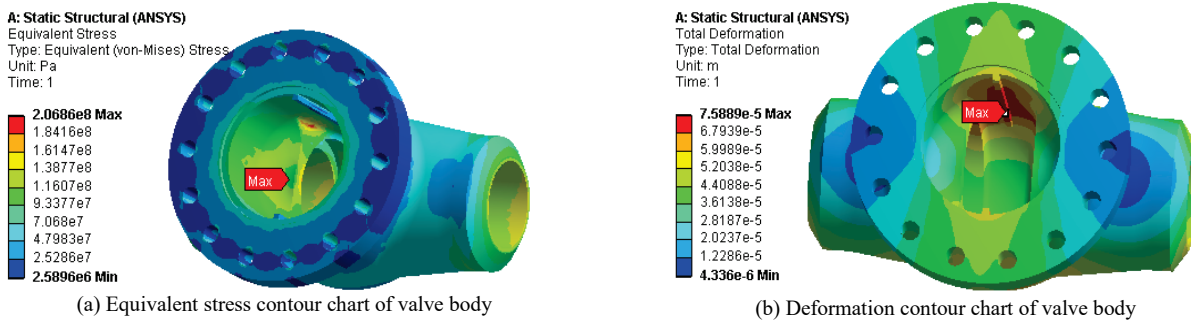(b) Deformation contour chart of valve body

Figure 14. Equivalent stress and deformation contour chart of Scheme 3
Source: The Authors.

The results before and after the valve body structure optimization are listed in Table 5. All the three schemes meet the relevant strength and stiffness requirements. The maximum equivalent stress of Scheme 1 is the largest and its maximum deformation and mass are the smallest among the three schemes. The maximum deformation of Scheme 2 is the largest; the maximum equivalent stress of Scheme 3 is the smallest and its mass is the largest. The maximum equivalent stress of the three optimization schemes was 4.5%, 5.2%, and 5.6% lower than that of the original scheme, respectively. Scheme 2 is a negative optimization in regards to maximum deformation. The maximum deformation of Scheme 1 was reduced by 2.6% and the maximum deformation of Scheme 3 remained unchanged. The mass values of schemes 1 and 2 were less than that of the original scheme, while that of Scheme 3 was higher.

Table 5.
Comparison of the results before and after the improvement of the valve body structure.

Design variable /mm	Initial scheme	Scheme1	Scheme2	Scheme3
D_1	115	113	114	116
D_2	160	162	162	162
D_3	59	60	58	59
D_4	50	51	49	50
D_5	12	12	14	15
Maximum equivalent stress /MPa	219.2	209.4	207.9	206.9
Maximum deformation /mm	0.076	0.074	0.078	0.076
Mass/kg	226.3	224.5	225.4	232.1

Source: The Authors.

The maximum equivalent stress, maximum deformation, and mass of Scheme 1 all decreased to varying extent compared with the original scheme. The maximum deformation of Scheme 2 and the mass of Scheme 3 comparatively increased, making their optimization effects inferior to those of Scheme 1.

7.5. Fluid-solid thermal coupling analysis of gate valve

The gate valve model was divided into an unstructured grid with 366033 units and 903515 nodes. A pressure of 15 MPa and temperature of 330 °C were applied to the inlet of the gate valve as a force of 80000 N was applied to the center flange bolt hole. The external surface of the gate valve was in contact with the air at this point and the heat transfer strength was low, so the convective heat transfer coefficient was set to 5 W/(m2·K). A fixed constraint was imposed on the left and right ends of the pipe.

The gate valves in this setup are mainly composed of the valve body, flashboard, valve stem, valve cover, filler, and other components, all of which bear the fluid and temperature loads. The heat source is an important boundary condition for solving the temperature field; the heat source of the gate valve temperature field is the fluid. The temperature and heat flow distribution of the Scheme 1 gate valve is shown in Fig. 15. The temperature and fluid are basically the same as the inlet and gate are in contact with the fluid. The temperature of the other parts gradually decreased over the course of this analysis. The heat flow of the valve seat and the middle flange was large and the temperature gradient was also large, which caused substantial thermal stress.

The deformation of the Scheme 1 gate valve is shown in Fig. 16 and Fig. 17. The gate valve deformed to the right under high-temperature and high-pressure fluid loads because the ends of the pipe were fixed. This can also be attributed to the thermal expansion caused by the high temperature. The maximum deformation of the gate valve was about 1.82 mm and located at the top of the stem. The maximum deformation of the gate was 0.78mm and located at the lower end of the gate.

The equivalent stress distributions of the Scheme 1 gate valve is shown in Fig. 18-20. Due to the pressure and temperature of the fluid, the stress was high at the inlet section, valve seat, and gate. The maximum equivalent stress was 143.14 MPa and located in the gate chamfer, where the stress concentration can be clearly observed. The maximum equivalent stress of the valve body was 92.76 MPa and located at the chamfering of the seat.

(a) Temperature distribution of gate valve
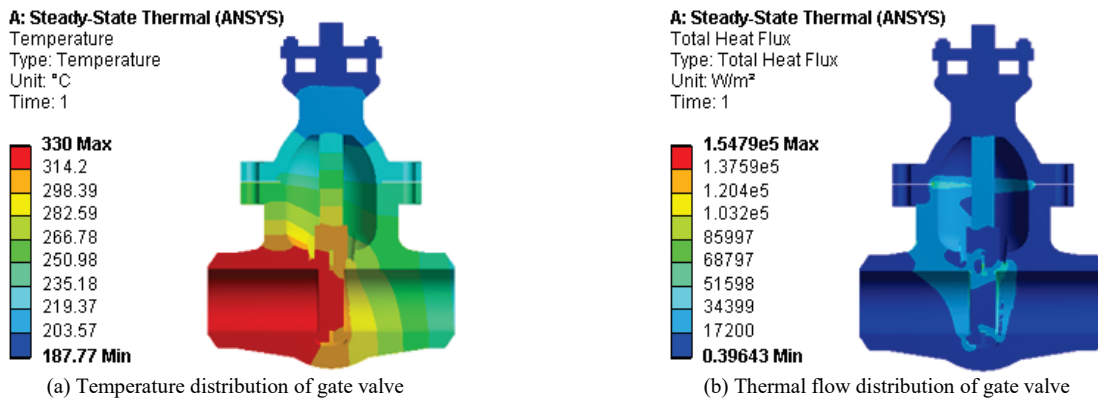

(b) Thermal flow distribution of gate valve

Figure 15. Temperature and thermal flow distribution of gate valve.
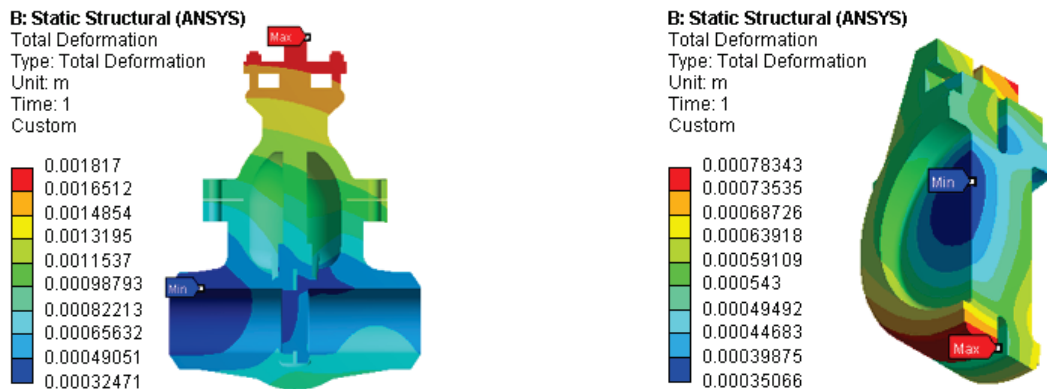Source: The Authors.

Figure 16. Deformation distribution of gate valve.
Source: The Authors.

Figure 17. Deformation distribution of gate.
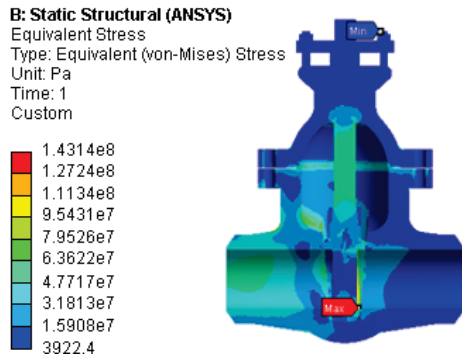Source: The Authors.

156

Figure 18. Equivalent stress distribution of gate valve.
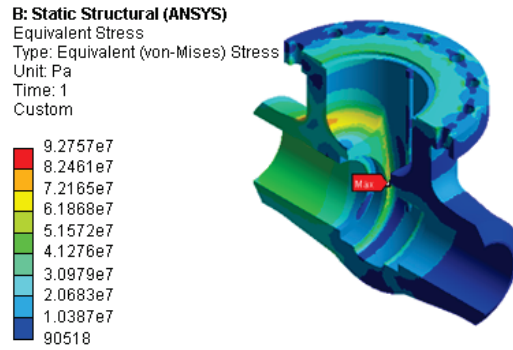Source: The Authors.

Figure 19. Equivalent stress distribution of valve body.
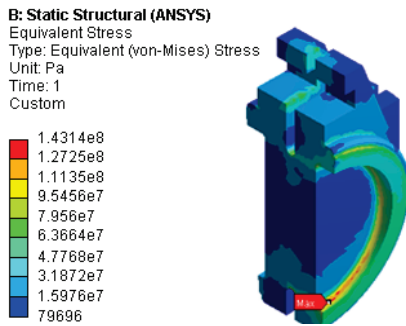Source: The Authors.

Figure 20. Equivalent stress distribution of gate.
Source: The Authors

The maximum equivalent stress of Scheme 1 under the closed state of the gate valve was 143.14 MPa, the maximum equivalent stress of Scheme 2 was 143.6 MPa, and the maximum equivalent stress of Scheme 3 was 144.25 MPa. The maximum equivalent stress of Scheme 1 is the smallest, Scheme 2 is the second, and Scheme 3 is the largest. The maximum equivalent stress of the three schemes did not markedly differ and the positions were the same. The maximum deformation of the gate valve and maximum equivalent stress of the gate were also very small.

The analysis indicates that all three gate valve designs meet the given stress requirements and have very small stress and deformation distribution and size. Scheme 1 is preferable in regards to its smallest stress and mass properties by comparison to Schemes 2 and 3.

8. Conclusions

The results of this study can be summarized as follows.

(1) The strength and stiffness of the initial nuclear valve can be calculated by finite element analysis and to determine the size and distribution of the deformation and equivalent stress under test pressure and working pressure conditions. Under 37.5 MPa test pressure, the stress concentration is located in the chamfer of the valve seat and the maximum equivalent stress of the valve body is 219.2 MPa, which exceeds the permissible stress of the material and indicates that the strength does not meet the design requirements.

Under 25 MPa working pressure, the valve body meets stiffness and strength requirements but the stress concentration at the chamfering of the seat part persists. It is necessary improve the stress concentration position in the valve body to enhance the safety and economy of the device.

(2) The structure of the valve body was optimized by testing three optimization schemes per their effects on the stress and deformation of the valve body. The maximum equivalent stress of Scheme 1 is the largest and its maximum deformation and mass are smallest among the three schemes. The maximum deformation of Scheme 2 is the largest. The maximum equivalent stress of Scheme 3 is the smallest and its mass is the highest. The optimization scheme improves the stress distribution of the valve body and decreases the stress at the original stress concentration point while making the stress distribution more uniform. This provides a theoretical basis for improving the entire valve body structure.

(3) Numerical calculations and fluid-solid thermal coupling analysis of the main over-flow and pressure-bearing parts in the closed gate valve were conducted to optimize the structure of the valve. The gate valve structure (with all three schemes) meets the given stress and deformation requirements under the working conditions. The difference between the sizes is very small across the three schemes; the stress and mass of Scheme 1 are the smallest.

References

[1]   Jianrui, L. et al., Design and numerical simulation of high-pressure nuclear power flat gate valve, Journal of Irrigation and Drainage Machinery Engineering, [online]. 30(5), pp. 573-577, 2012. (in Chinese). Available at: DOI: zzs.edu.cn/pgjx/EN/abstract/abstract450.shtml.

[2]   Yu X., Chen S., Yang, X, et al., Numerical and experimental study on characteristics of pressure relief valve in large irrigation pipe network[J], Journal of Drainage and Irrigation Machinery

Engineering, [online]. 36(09), pp. 824-829, 2018. (in Chinese). Available at: https://kns.cnki.net/kcms/detail/detail.aspx?dbcode= CJFD&filename=PGJX201809010&dbname=CJFDLAST2018.

[3] Jianrui, L. et al., Fluid-solid thermal coupling analysis of high temperature and high-pressure gate valve, Fluid Machinery, [online]. 3, pp.16-20, 2012. (in Chinese). Available at: https://kns.cnki.net/kcms/detail/detail.aspx?dbcode=CJFD&filename =LTJX201203003&dbname=CJFD2012.

[4] Zhou, D., Jiang S., Chen H. et al., Numerical simulation of start-up process of mixed flow pump unit combined with hydraulic control butterfly valve action[J], Journal of Drainage and Irrigation Machinery Engineering (JDIME), [online]. 37(02), pp. 112-117, 2019. (in Chinese) Available at: DOI: en.cnki.com.cn/Article_en/CJFDTotal-PGJX201902002.htm.

[5] Yin, T., Pei, J., Yuan, S. et al. Fluid-structure interaction analysis of an impeller for a high-pressure booster pump for seawater desalination. J. Mech. Sci. Technol 31, pp. 5319-5328, 2017. DOI: 10.1007/s12206-017-1026-z.

[6] Yusuke, S. et al., Development of bellows and gate valves with a comb-type rf shield for high-current accelerators: four-year beam test at KEK B-Factory, Review of Scientific Instruments,78(4), pp. 1-7, 2007. DOI: 10.1063/1.2723747.

[7] Hongchao, J. et al., Optimization of a pressure control valve for high power automatic transmission considering stability, Mechanical Systems and Signal Processing, 101, pp. 182-196, 2007. DOI: 10.1016/j.ymssp.2017.08.018.

[8] Samad, M. et al., Modeling of fluid-induced vibrations and identification of hydrodynamic forces on flow control valves, Journal of Central South University, 22(7), pp. 2596-2603, 2015. DOI: 10.1007/s11771-015-2789-y.

[9] Marek, A, and Okrajn, J., Local stress-strain behavior of a high-temperature steam valve under transient mechanical and thermal loading, Journal of Materials Engineering and Performance, 23(1), pp. 31-38, 2014. DOI: 10.1007/s11665-013-0744-3.

[10] Jianhui, Z. et al., Hold current effects on the power losses of high-speed solenoid valve for common-rail injector, Applied Thermal Engineering, 128, pp. 1579-1587, 2018. DOI: 10.1016/j.applthermaleng.2017.09.123.

[11] Liu, B., Zhao, J. and Qian, J., Numerical analysis of cavitation erosion and particle erosion in butterfly valve, Engineering Failure Analysis, 80, pp. 312-324, 2017. DOI: 10.1016/j.engfailanal.2017.06.045.

[12] Hu B. et al., Numerical investigation of conjugate heat transfer of an underwater gate valve assembly, Applied Ocean Research, 56, pp. 1-11, 2016. DOI: 10.1016/j.apor.2015.12.006.

[13] Zhe, L. et al., Influence of flashboard location on flow resistance properties and internal features of gate valve under the variable condition, Journal of Natural Gas Science and Engineering, 33, pp. 108-117, 2016. DOI: 10.1016/j.jngse.2016.05.025.

[14] Jianjun, H., Yuan, Z. and Dun, Z.., Hydraulic characteristics of the flow field of the pump sluice, Journal of Irrigation and Drainage Machinery Engineering, [online]. 28(2), pp. 149-154 2010. Available at: https//: en.cnki.com.cn/Article_en/CJFDTotal-PGJX201002014.htm

[15] Zhe, L. et al., Effect of placements (horizontal with vertical) on gas-solid flow and particle impact erosion in gate valve, Journal of Thermal Science, 23(6), pp. 558-563, 2014. DOI: 10.1007/s11630-014-0741-3.

[16] Tomarov, G.V., Shipkov, A.A. and Koreshkova, N.S., Calculated and experimental substantiation of operating conditions under which adequate erosion resistance of valves used in power units at nuclear power stations is ensured, Thermal Engineering, 57(5), pp. 382-390, 2010. DOI: 10.1134/s0040601510050046.

[17] Kolesnikov, G.N. and Tikhonov, E.A., Contact interaction between seat and wedge in gate valves, Chemical & Petroleum Engineering, 50(5-6), pp. 382-386, 2014. DOI: 10.1007/s10556-014-9911-0.

[18] Hao, W., Noureddine bensseddiq and abdellatif imad. Fracture toughness prediction of a valve body: numerical analysis, Engineering Failure Analysis, 17(1), pp. 135-142, 2010. DOI: 10.1016/j.engfailanal.2009.04.010.

[19] Bai, M., Wang, F., Lei, C. et al. Effect of bypass valve on hydraulic transient process in long water transport pipelines with gravity flow[J]. Journal of Drainage and Irrigation Machinery Engineering

(JDIME), 37(01), pp. 58-62, 2019. (in Chinese) DOI: zzs.ujs.edu.cn/pgjx/CN/article/searchArticle.do.

[20] Wang, X., Li, X., Shen, Z. et al., Finite element simulation on investigations, modeling, and multiobjective optimization for clinch joining process design accounting for process parameters and design constraints[J]. The International Journal of Advanced Manufacturing Technology, 96, pp. 3481-3501, 2018. DOI: 10.1007/s00170-018-1708-4

[21] Zhou, L., Bai, L., Shi, W. et al., Numerical analysis and performance experiment of electric submersible pump with different diffuser vanes number. J. Braz. Soc. Mech. Sci. Eng., 40, art. #89, 2018. DOI: 10.1007/s40430-018-0986-y.

[22] Daoxing, Y., Xide, L., Hong, L. et al., Optimal design and experiment of exhaust vent on impeller of medium consistency pulp pump[J]. Advances in Mechanical Engineering, 10(3), pp. 168781401876555, 2018. DOI: 10.1177/1687814018765557

W. Li, is Dr. of engineering, researcher, doctoral supervisor. Deputy director of Research Center of Fluid Machinery Engineering and Technology in Jiangsu University. Mainly engaged in the design, optimization and dynamic stability of fluid machinery (pump).
ORCID: 0000-0003-1130-4336

E. Li, is MSc. He is studying in Research Center of Fluid Machinery Engineering and Technology in Jiangsu University and engaged in research of fluid machinery.
ORCID: 0000-0002-0755-2831

H. Chang, is Dr. He is studying in Research Center of Fluid Machinery Engineering and Technology in Jiangsu University and engaged in research of fluid machinery.
ORCID: https://orcid.org/0000-0002-5953-7692

J. Liu, is professor level senior engineer. He is working in Research Center of Fluid Machinery Engineering and Technology in Jiangsu University and engaged in research of fluid machinery.
ORCID: https://orcid.org/0000-0002-6902-3740

Ch. Li, is MSc. He is studying in Research Center of Fluid Machinery Engineering and Technology in Jiangsu University and engaged in research of fluid machinery.
ORCID: https://orcid.org/0000-0003-0739-4105

X. Wang, is MSc, and Eng. He is working in Kunming Branch of 705 Research Institute and engaged in research of fluid machinery.
ORCID: https://orcid.org/0000-0002-2578-6703